Improved Human-Robot Collaborative Control of Redundant Robot for Teleoperated Minimally Invasive Surgery

Hang Su[1], Chenguang Yang[2], Giancarlo Ferrigno[1] and Elena De Momi[1]

***Abstract*—An improved human-robot collaborative control scheme is proposed for a teleoperated Minimally Invasive Surgery (MIS) scenario, based on a hierarchical operational space formulation of a 7 DoF redundant robot. The redundancy of the manipulator is exploited to guarantee a remote center of motion (RCM) constraint and to provide a flexible workspace for the medical staff to assist physicians, supports patients, etc. Based on the implemented hierarchical control framework, an RCM constraint and a safety enhanced constraint are applied to the null-space motion to achieve the teleoperated minimally invasive surgical tasks with human-robot interaction. Due to the physical interactions, issues with safety and accuracy of the surgical task execution may arise. The control framework integrates adaptive compensators to guarantee the accuracy of the surgical tasks and to maintain the RCM constraint in a decoupled way with uncertain physical interactions. The performance of the proposed algorithm is verified with virtual surgical tasks in a patient phantom. Compared with the methods proposed in the literatures, it can be concluded that both the accuracy of the end-effector and the RCM constraint are improved. The compliant null-space motion is also constrained in a safe area, and the interaction force on the abdominal wall is converged into a smaller area.**

***Index Terms*—Physical Human-Robot Interaction; Redundant Robots; Surgical Robotics: Laparoscopy**

I. INTRODUCTION

FOR teleoperated Minimally Invasive Surgery (MIS), the end-effector of the surgical tip must go through small incisions on the patient's abdominal wall. It is important to assure that the tool should not apply big forces on the incision wall in order to prevent patient harm. Hence each small incision produces a kinematic constraint, commonly known as the RCM constraint [1][2], as shown in Fig. 1.

Maintaining the Remote Center of Motion (RCM) constraint safely without any loss of accuracy of the surgical tip has always been a challenging task and has attracted towards increasing research interest in recent years. In general, the RCM constraint can be active or passive. The passive constraint is mechanically maintained by utilizing spherical mechanisms or by dual-parallelograms design and the passive joints guarantee that no forces are exerted to the entry point, while the active way is known to achieve the RCM constraint directly with a software controller [3]. Parallel-type robots, such as the *da Vinci* surgical system and the *AESOP* manipulator, are specifically designed to passively achieve the motion [4]. Whereas, open-chained manipulators, such as the DLR MIRO robots, usually adopt the motion controller to maintain the RCM constraint [5]. Compared with the passive way, the active way is more popular in the non-clinical research [3][6][7], since it provides a lot of benefits, like economic feasibility and task-space flexibility. Ortmaier *et al.* implemented an inverse kinematic control to achieve RCM constraint motion, preventing any force exerted on the trocar during the minimally invasive robotic surgery scenario [8] without using high-cost mechanisms to achieve the constraint. In our previous work [7][9], we solved the RCM constraint in the task space and implemented a Cartesian impedance controller to control it in an active way.

High contact forces may emerge in case of a rigid interaction[10][11], which can be dangerous for the surgical operation. Impedance control is an efficient way to avoid rigid interaction and force overshoots. However, most of the work did not consider and analyze the physical interaction force between the tool shaft and the abdominal wall on the RCM constraint.

Redundancy of the serial manipulators can be exploited to achieve additional tasks, for example, obstacle avoidance [12] and human-like behavior [13]. It is effective to utilize the redundancy to maintain the active RCM constraint. Sandoval *et al.* proposed an improved dynamic control approach to utilize the redundancy for RCM constraint [6]. In our previous work, the redundancy was utilized to provide flexible workspace [7][14] and an adaptive decoupling controller [15] was applied to achieve the RCM constraint. Furthermore, we utilize the redundancy to provide flexible workspace with compliant motion behavior for the nurse or the surgeon to assist physicians or to support the patients [7][9]. A safety enhanced controller is proposed to guarantee a correct task execution and a constrained compliant behavior of the robot's body in case of accidental interaction in the null-space, and introduce direct fuzzy adaptive approximation [16][17] to compensate

Manuscript received: September, 7, 2018; Revised December, 2, 2018; Accepted December, 31, 2018.

This paper was recommended for publication by Editor Allison M. Okamura, upon evaluation of the Associate Editor and Reviewers' comments. *This work was supported by the European Unions Horizon 2020 research and innovation program under SMARTsurg project grant agreement No. 732515. This work was partially supported by Engineering and Physical Sciences Research Council (EPSRC) under Grant EP/S001913/1.

[1]Hang Su, Giancarlo Ferrigno and Elena De Momi are with the Department of Electronics, Information and Bioengineering, Politecnico di Milano, 20133, Milan, Italy. hang.su, giancarlo.ferrigno, elena.demomi@polimi.it

[2]Chenguang Yang is with Bristol Robotics Laboratory, University of the West of England, Bristol, BS16 1QY, UK. cyang@ieee.org

Digital Object Identifier (DOI): see top of this page.

the disturbance from human-robot interaction in [9].

However, the previous strategies solve the RCM constraint with trajectory planning in the task space without decoupling, which influences the accuracy of the surgical tip. Dietrich *et al.* introduced a Hierarchical Operational Space combining multiple null-space controllers and proved its stability [18][19], making it possible to solve the RCM constraint and the compliant swivel behavior with hierarchical null-spaces in a single controller. In this paper, we utilize the hierarchical operational space formulation [19] to achieve the whole-body impedance control of a 7-DoF serial robot. The surgical task implementation in [9] is improved with our novel strategy by achieving RCM constraint in its first lower-priority task in the 1^{st} Null-space of the Jacobian matrix of the surgical tip. And we put the safety-enhanced compliant arm behavior as a second lower-priority task in the 2^{nd} Null-space of the Jacobian matrix of the RCM constraint. Furthermore, we introduce a decoupled fuzzy compensator to compensate the disturbances and improve the accuracy of the surgical tip and the RCM constraint, improving the human-robot collaborative control in teleoperated MIS. A comparison of methods experiment is performed to validate the proposed control method by using the LWR4+ (KUKA, Germany) and Sigma 7 (Force dimension, Switzerland) in a lab setup environment.

This paper is organized as follows: Methodology is presented in Section II. In Section III, the performance of the proposed control schemes is evaluated in a lab setup environment. Finally, conclusions are drawn in Section IV.

II. Methodology

A. Prior work

1) Modeling of the Serial Robot: The dynamic model of an n degree of freedom (DoF) serial manipulator can be expressed as [20]:

$$\boldsymbol{M(q)\ddot{q} + C(q,\dot{q})\dot{q} + g(q) - \tau_e = \tau_C} \tag{1}$$

where $\boldsymbol{q} \in R^n$ is the joint values vector, $\boldsymbol{M(q)} \in R^{n\times n}$ is the inertia matrix, which is bounded and symmetric positive definite, $\boldsymbol{C(q,\dot{q})} \in R^{n\times n}$ is a matrix representing the Coriolis and Centrifugal effects, and $\boldsymbol{g(q)} \in R^n$ is the vector of gravity torques. The torque vectors $\boldsymbol{\tau_C} \in R^n$ and $\boldsymbol{\tau_e} \in R^n$ represent the control torques and the external disturbance torque vectors respectively. For simplification, we assume that the robot is far away from its singularity and the pseudoinverse of its Jacobian matrix $\boldsymbol{J_T(q)} \in R^{m\times n}$ exists.

Since the desired behavior of the serial robot in the teleoperated MIS is expressed in the task space, the above generalized formulation can be rewritten as follows [21][22]:

$$\boldsymbol{M_X(X)\ddot{X} + H_X(X,\dot{X})\dot{X} + J_T^{-T}(q)g(q) - F_{eT} = F} \tag{2}$$

where $\boldsymbol{X} \in R^m$ is the task space coordinates vector and $\dot{\boldsymbol{X}} \in R^m$ is the actual Cartesian velocity,

$$\boldsymbol{M_X(X)} = \boldsymbol{J_T^{-T} M(q) J_T^{-1}} \tag{3}$$

$$\boldsymbol{H_X(X,\dot{X})} = \boldsymbol{J_T^{-T}[C(q,\dot{q}) - M(q)J^{-1}\dot{J}_T]J_T^{-1}} \tag{4}$$

$$\boldsymbol{F_{eT}} = \boldsymbol{J_T^{-T}\tau_e} \tag{5}$$

The matrix $\boldsymbol{M_X(X)} \in R^{m\times m}$ is the Cartesian inertia matrix, $\boldsymbol{H_X(X,\dot{X})} \in R^{m\times m}$ is the Cartesian Coriolis and Centrifugal force effects, $\boldsymbol{F_{eT}} \in R^m$ is the external force vector in task space, with

$$\exists \beta \in R, \|\boldsymbol{F_{eT}}\| \le \beta, \forall t \ge 0 \tag{6}$$

Property 2.1: The Cartesian inertia matrix $\boldsymbol{M_X(X)}$ as defined in (3) is symmetric and positive, which can be bounded as:

$$\lambda_1\|\boldsymbol{A}\| \le \boldsymbol{A^T M_X(X) A} \le \lambda_2\|\boldsymbol{A}\|, \forall \boldsymbol{A}, \boldsymbol{X} \in R^m \tag{7}$$

where $\lambda_1 \in R$ and $\lambda_2 \in R$ are positive constants.

Property 2.2: The Coriolis and Centrifugal force matrix $\boldsymbol{H_X(X,\dot{X})}$ and the time derivative of the Cartesian inertia matrix $\boldsymbol{M_X(X)}$ satisfy

$$\boldsymbol{A^T[\dot{M}_X(X) - 2H_X(X,\dot{X})]A} = 0, \forall \boldsymbol{A}, \boldsymbol{q}, \dot{\boldsymbol{q}} \in R^n \tag{8}$$

2) Hierarchical Operational Space Formulation:

$$\boldsymbol{\dot{X} = J_T(q)\dot{q}} \tag{9}$$

where $\boldsymbol{J_T(q)} \in R^{m\times n}$ is the Jacobian matrix from the base frame to the end-effector. Since the number of the degrees of freedom is greater than $m = 3$, the redundancy of the serial robot could be utilized to achieve additional tasks. Extended Jacobian method [23] is introduced to enrich the task space including both the end-effector and the null-space kinematic coordination. The corresponding control law of the extended dynamical formulation can be written as [22][24]:

$$\boldsymbol{F_T = M_X\ddot{X}_d + H_X\dot{X}_d - K_X(X - X_d) - D_X(\dot{X} - \dot{X}_d)} \tag{10}$$

$$\boldsymbol{F_{N_1} = -K_{N1}(N_1 - N_{1d}) - D_{N1}(\dot{N}_1 - \dot{N}_{1d})} \tag{11}$$

$$\boldsymbol{F_{N_2} = -K_{N2}(N_2 - N_{2d}) - D_{N2}(\dot{N}_2 - \dot{N}_{2d})} \tag{12}$$

where $\boldsymbol{F_T} \in R^3$ is the active force in task space. $\boldsymbol{F_{N1}}$, $\boldsymbol{F_{N2}}$ are the forces applied on the null-space kinematics. $\boldsymbol{N_1}$,$\boldsymbol{N_2}$ are the actual null-space coordinates vectors. $\boldsymbol{N_{1d}}$,$\boldsymbol{N_{2d}}$ are the corresponding desired null-space coordinates vectors. Finally, the null-space force can be mapped into joints torque using the null-space controller ($\boldsymbol{\tau_N} \in R^n$), which is defined as:

$$\boldsymbol{\tau_N = (I - J_T^T(q)J_T(q)_M^+)J_N^T F_N} \tag{13}$$

where $\boldsymbol{J_N} \in 3^{n-m}$ is Jacobian matrix from the base frame to the null-space kinematics, and $\boldsymbol{J_T(q)_M^+}$ is the inertia-weighted pseudo-inverse matrix [21]:

$$\boldsymbol{J_T(q)_M^+ = (J_T(q)M(q)^{-1}J_T(q)^T)^{-1}J_T(q)M(q)^{-1}} \tag{14}$$

The corresponding control diagram is shown in Fig. 2 and the stability analysis are verified in [22][24].

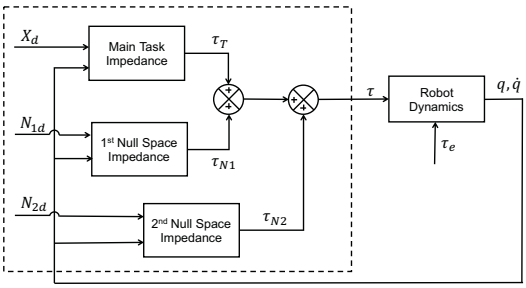

Fig. 2. Block diagram representing the hierarchical control architecture.

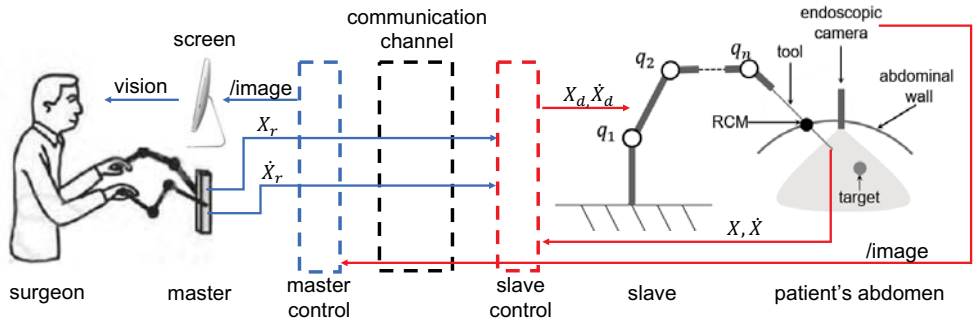

Fig. 1. Typical teleoperated Minimally Invasive Surgery structure. $\boldsymbol{X_r, \dot{X}_r} \in R^m$ are the desired Cartesian position and velocity in the master frame, respectively. $\boldsymbol{X, \dot{X}} \in R^m$ are the actual Cartesian position and velocity in the slave frame, respectively. $\boldsymbol{X_d, \dot{X}_d} \in R^m$ are the desired Cartesian position and velocity in the slave frame, respectively

3) Teleoperated Surgical Task Implementation: As it is shown in Fig. 3, the interaction force $\boldsymbol{F_e}$ between the surgical tool shaft and the abdominal wall should be minimized during the teleoperated surgery to avoid increasing the invasive wound. To drive the end-effector position ($\boldsymbol{X} \in R^3$) reaching the desired position ($\boldsymbol{X_r} \in R^3$) from the master, an interpolation method is introduced to reach the desired position smoothly as [25]:

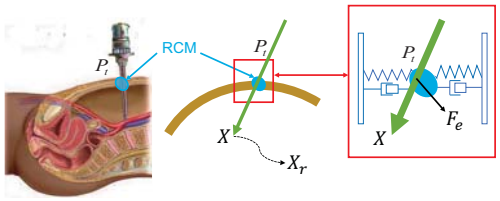

Fig. 3. Tele-operated MIS surgical scene: During the surgery, the tool shaft must go through the trocar position P_t, representing the RCM Constraint, where X and X_r are the actual and desired Cartesian position inside the abdomen, F_e is the interaction force between the surgical tool shaft and the abdominal wall.

$$\boldsymbol{X_d} = -k_0(\boldsymbol{X} - {}^s\boldsymbol{T_m}\boldsymbol{X_r}) + {}^s\boldsymbol{T_m}\dot{\boldsymbol{X}}_{\boldsymbol{r}} \tag{15}$$

where ${}^s\boldsymbol{T_m}$ is the transformation matrix from the master frame to the slave frame, $k_0 > 0$ is a positive coefficient. Then a Cartesian compliance control term, $\boldsymbol{\tau_T} \in \boldsymbol{R^7}$, defined in our previous work [7][9], is introduced to achieve impedance control of the surgical tip.

4) Safety-enhanced Compliant Arm Behavior: The surgical tip was utilized to perform surgical tasks and the RCM constraint, the swivel angle $\psi \in R$ of the robot arm, defined in [26], was left as the kinematic redundancy. In our previous work [7][9], a safe swivel motion constraint $[\psi_{minf}, \psi_{maxf}]$ is defined, which is assumed to depend on the actual situation in the operating room, and a virtual force $\boldsymbol{F_\psi}$ is defined to prevent the swivel motion exceed the swivel boundary.

B. Control System Development

The prior work hierarchical operational space formulation is introduced to integrate the teleoperated surgical task implementation and the safety-enhanced compliant arm behavior in our previous work [7][14]. The surgical task implementation in [9] is improved with our novel strategy by achieving RCM constraint in its first lower-priority task in the 1^{st} Null-space of the Jacobian matrix of the surgical tip. And we put the safety-enhanced compliant arm behavior as a second lower-priority task in the 2^{nd} Null-space of the Jacobian matrix of the RCM constraint. Then we introduce the novel decoupled adaptive fuzzy compensation to enhance both the accuracy for the surgical tip and the RCM constraint. Details are listed as follows:

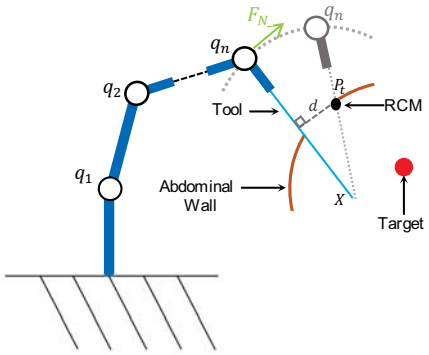

Fig. 4. Achieve RCM constraint with null-space controller: d is the distance between the trocar position ($\boldsymbol{P_t}$) and the tool (the small incision is zoomed for a better understanding). The actual tool-tip position $\boldsymbol{X}$ is controlled by teleoperation to reach the target in the patient's abdomen, $\boldsymbol{F_N}$ is the virtual force applied to the 1^{st} null-space of the task space.

1) RCM Constraint in the 1^{st}Null-space: To guarantee that the tool shaft always goes through the trocar position, the RCM constraint distance error $d = \|(\boldsymbol{P_t} - \boldsymbol{X}) \times \hat{\boldsymbol{u}}_{\boldsymbol{c}}\| \in R$ is defined in Fig. 4, where $\hat{\boldsymbol{u}}_{\boldsymbol{c}} \in R^3$ is the unit direction vector of the actual surgical tip pose. To satisfy the constraint without having any influence on the main surgical task, the safer solution is to drive the last joint "wrist" (q_n) tracking a circular movement around the end-effector from the actual position $\boldsymbol{N_1}$ to the desired position $\boldsymbol{N_{1d}}$ until the tool shaft passes through the trocar position $\boldsymbol{P_t}$, as shown in Fig. 4. Accordingly, the grey joint q_n is viewed as the desired position ($\boldsymbol{N_{1d}}$) of the last joint. Hence, the RCM controller can be introduced as:

$$\boldsymbol{F_N} = -\boldsymbol{K_N}\boldsymbol{e_{N1}} - \boldsymbol{D_N}\dot{\boldsymbol{e}}_{\boldsymbol{N1}} \tag{16}$$

where $\boldsymbol{K_N, D_N} \in R^3$ are the corresponding stiffness and damping matrix, $\dot{\boldsymbol{N}}_1$ is the actual velocity of the "wrist" and $\boldsymbol{e_N = N_1 - N_{1d}}$ is the tracking error. Since $\boldsymbol{||e_N||}$ is proportional to the RCM constraint error $\boldsymbol{d}$: $\boldsymbol{d = \lambda ||e_{N1}||}, 0 < \boldsymbol{\lambda} \leq 1$. Hence, $\boldsymbol{e_{N1} = (P_t - X) \times \hat{u}_c/\lambda}$. The first null-space controller can introduced as:

$$\boldsymbol{\tau_{N_{11}} = (I - J_T^T(q) J_T(q)_M^+) J_W^T F_N} \tag{17}$$

where $\boldsymbol{J_W(q)} \in R^{3\times5}$ is the Jacobian matrix from the base frame to the robot wrist. In general, λ varies according to the tip position during the teleoperation. In this paper, we choose λ as a constant, but we resolve the time-varying system with fuzzy compensator in the following steps.

2) Constrained Compliant Behaviour in the 2^{nd} Null-space: The 2^{nd} null-space controller, introduced in our previous work [7][9], is defined as:

$$\boldsymbol{\tau_{N_2} = (I - J_W^T(q) J_W(q)_M^+) J_E^T F_\psi} \tag{18}$$

where $\boldsymbol{J_E(q)} \in R^{3\times3}$ is the Jacobian matrix from the base to the robot elbow.

3) Decoupled adaptive fuzzy compensation for uncertain disturbances with physical interaction: Since there is a physical interaction between the surgical tool shaft and the patient's abdominal wall, as shown in Fig. 3. It should also be mentioned that the tissue characteristic discrepancies exist and vary between different patients [27][28]. The dynamics of $\boldsymbol{F_e}$ is unknown and nonlinear in a real clinical application and has been introduced for analysis. Furthermore, the hand force $\boldsymbol{F_H}$, shown in Fig. 6, applied on the robot arm [7][9] is also uncertain and time-varying. It is known that $\boldsymbol{F_e}$ and $\boldsymbol{F_H}$ can be decomposed into two components influencing the accuracy of the surgical tip and the RCM constraint, separately. The implementation of the surgical task could be viewed as controlling the surgical tip regarding external disturbances.

The approximation of a nonlinear disturbance $\boldsymbol{f(Z)} : R^n \rightarrow R^m$ can be represented as follows:

$$\boldsymbol{f(Z) = \theta^T S(Z) + \varepsilon(Z)} \tag{19}$$

where the vector $\boldsymbol{Z} = [z_1, z_2, ..., z_n] \in R^n$ is the input vector of the approximators, and $\boldsymbol{S(Z)} \in R^l$ is a chosen linear or nonlinear basis function, $\boldsymbol{\theta} \in R^l$ is a vector of adaptable weights, and $\varepsilon \in R$ is the approximation error which is bounded over the compact set, meeting the condition: $\exists \bar{\varepsilon} \in R^+, |\varepsilon(\boldsymbol{Z})| \leq \bar{\varepsilon}, \forall \boldsymbol{Z} \in \boldsymbol{\Omega}_Z$. In this paper, the FLS rule [29][30][31]is chosen by

$$\xi_j = \frac{\prod_{i=1}^n \mu_{A_i^l(z_i)}}{\sum_{j=1}^m \prod_{i=1}^n \mu_{A_i^l(z_i)}}, \ j = 1, \ldots, m \tag{20}$$

The adaptive control law [9] to adjust the weight parameters $\boldsymbol{\Theta}$ is chosen as $\dot{\boldsymbol{\Theta}} = [\dot{\boldsymbol{\theta}}_1, \dot{\boldsymbol{\theta}}_2, ..., \dot{\boldsymbol{\theta}}_m] \in R^{m\times l}$, $\dot{\boldsymbol{\theta}}_i \in R^l, i = 1, 2, ..., m$:

$$\dot{\boldsymbol{\theta}}_i = \begin{cases} \boldsymbol{\gamma e_i P \xi^T(Z)}, & \boldsymbol{||\theta_i|| < M_{\theta_i}} \text{ or } (\boldsymbol{||\theta_i|| \geq M_{\theta_i}} \\ & \boldsymbol{\& \ \gamma E P \xi^T(Z) < 0}). \\ \boldsymbol{\Gamma(Z)}, & \boldsymbol{||\theta_i|| \geq M_{\theta_i} \& \ \gamma e_i P \xi^T(Z) \geq 0}. \end{cases} \tag{21}$$

where $\boldsymbol{\Gamma(Z)} = \boldsymbol{\gamma e_i P (1 - \frac{\theta_i \theta_i^T}{||\theta_i||^2}) \xi^T(Z)}$, and $\boldsymbol{\gamma} \in R^{m\times m}$ is a diagonal matrix determining the updating speed, $\boldsymbol{E} = [\boldsymbol{e_1, e_2, ..., e_m; \dot{e}_1, \dot{e}_2, ..., \dot{e}_m}]^T \in R^{m\times2}$ is the system output error vector, and $\boldsymbol{P} \in R^{2\times1}$ is the last column of a symmetric positive definite matrix based on the Lyapunov function [32]. We adopted the following decoupled compensator to approximate the disturbance on the end-effector and the RCM constraint, separately. The input of FLS rule is desired position, desired velocity, actual position, and actual velocity. The output of FlS is the impedance force on each axis. To approximate the extern disturbances:

$$\boldsymbol{\tau_{T_2}} = \boldsymbol{J_T \theta_X^T S(X)} \tag{22}$$

$$\boldsymbol{\tau_{N_{12}}} = \boldsymbol{(I - J_T^T(q) J_T(q)_M^+) J_W \theta_N^T S(N)} \tag{23}$$

where $\boldsymbol{E_T = [X - X_d; \dot{X} - \dot{X}_d]^T} \in R^{3\times2}$ and $\boldsymbol{E_N = [e_{N1}; \dot{e}_{N1}]^T} \in R^{3\times2}$.

The overview of proposed improved human-robot collaborative control (IHRCC) block diagram is shown in Fig. 5. The desired control term can be expressed as:

$$\boldsymbol{\tau_d = \tau_{T_1} + \tau_{T_2} + \tau_{N_{11}} + \tau_{N_{12}} + \tau_{N_2}} \tag{24}$$

4) System Description: The lab setup of the teleoperated MIS system is shown in Fig. 7. A redundant robot (LWR4+, KUKA, Germany) is torque-controlled through the Fast Research Interface (FRI) [33]. The teleoperation scheme implements a Cartesian position control for 3D coordinates with a master device (Sigma 7, Force Dimension, Switzerland) and a switch pedal [34]. An endoscopic camera HD and an ArUco maker board are used to create the virtual surgical tasks in augmented reality [35]. A 6-axis force sensor (M8128C6, SRI, China) is used to measure the interaction force between the surgical tool shaft and the abdominal wall on the RCM constraint. The description of the software system is in [7][9][14].

TABLE I
EXPERIMENTAL CONTROLLER PARAMETERS

Controller	Controller parameters
DCAC ($\boldsymbol{\tau_d = \tau_{T_1} + \tau_{N_{11}}}$)	$\boldsymbol{K_X} = diag[3000, 3000, 3000]$ $\boldsymbol{D_X} = diag[30, 30, 30]$ $\boldsymbol{K_N} = diag[800, 800, 800]$ $\boldsymbol{D_N} = diag[10, 10, 10]$, $\lambda = 0.5$
IHRCC ($\boldsymbol{\tau_d = \tau_{T_1} + \tau_{N_{11}}}$ $\boldsymbol{+\tau_{T_2} + +\tau_{N_{12}} + \tau_{N_2}}$)	$\boldsymbol{K_X} = diag[3000, 3000, 3000]$ $\mathbf{D_X} = diag[30, 30, 30]$ $\boldsymbol{K_N} = diag[800, 800, 800]$ $\boldsymbol{D_N} = diag[10, 10, 10]$, $\lambda = 0.5$ $k_0 = 0.1, k_\psi = 150.0, d_\psi = 5.0, \rho = 0.06$ $\boldsymbol{\gamma} = diag[0.3, 0.3, 0.3, 0.03, 0.03, 0.03]$ $\boldsymbol{P} = diag[14, 2]$ $\boldsymbol{M_\Theta} = [0.5, 0.5, 0.5, 0.5, 0.5, 0.5]$

III. EXPERIMENTAL DEMONSTRATION

Here we experimentally demonstrate the concept of the proposed control approach. One teleoperator (User 2) and one medical staff (User 1) were enrolled and the whole procedure [9] is shown in Fig. 8. The constraint swivel motion and the RCM constraint are validated with physical interaction, while the surgical tip is teleoperated to track virtual trajectories without physical interaction. The tool shaft should always go through the RCM constraint on the patient phantom during the teleoperation. The medical staff is free to move the robot

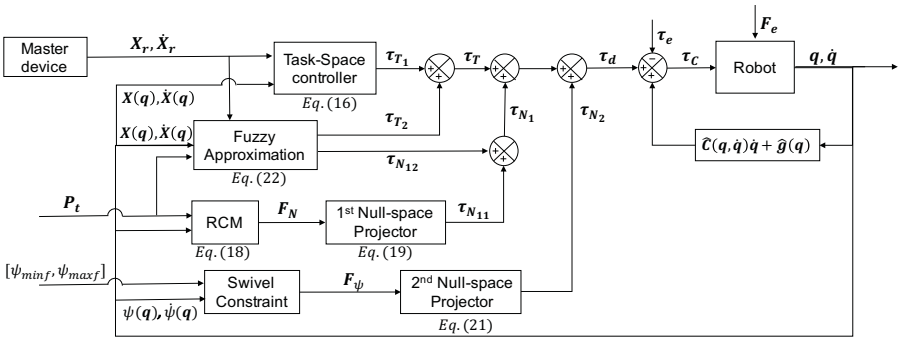

Fig. 5. Block diagram representing the proposed control architecture: The "Task-space controller" block is used to achieve the end-effector tracking. The "RCM" block and the "1^{st} Null-space Projector" are adopted to respect the RCM constraint, while the "Swivel Constraint" and the "2^{nd} Null-space Projector" calculates the virtual force applied on the 2^{nd} null-space, and the "Fuzzy Approximation" compensates the unknown disturbance in the task space and the 1^{st} null-space in a decoupled way. "Robot" is robot arm dynamic model with uncertain physical interaction.

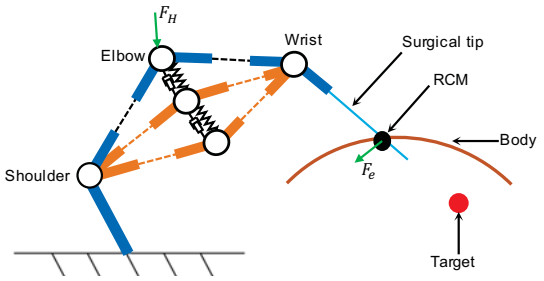

Fig. 6. Physical interaction and corresponding external disturbance: $\boldsymbol{F_H}$ is the human hand force on the elbow, and $\boldsymbol{F_e}$ is the external force generated by the interaction between the surgical tool shaft and the abdominal wall.

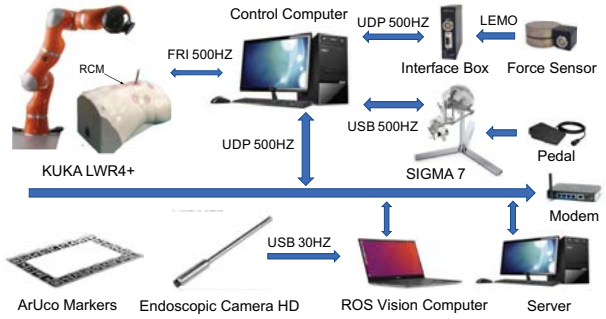

Fig. 7. Overview of the teleoperated surgical robot control system.

arm in an allowed swivel area with hands [9]. Virtual task paths were designed in the surgical space and overlaid on the camera image. The virtual task for teleoperation tracking is with different shapes [9]. The user 2, sitting at the remote desk and using the monitor to observe the scene, is asked to follow the line with the robot end-effector. The performed trajectory is overlaid on the camera image plane.

The magnitude of Cartesian position error, $\boldsymbol{E_X}$, the RCM constraint error, d, and the interaction force $\boldsymbol{F_e}$, shown in Fig. 9, are recorded to evaluate the proposed control method:

$$\|\boldsymbol{E_X}\| = \|\boldsymbol{X_d} - \boldsymbol{X}\| \tag{25}$$

$$d = \|(\boldsymbol{P_t} - \boldsymbol{X}) \times \hat{\boldsymbol{u}}_{\boldsymbol{c}}\| \tag{26}$$

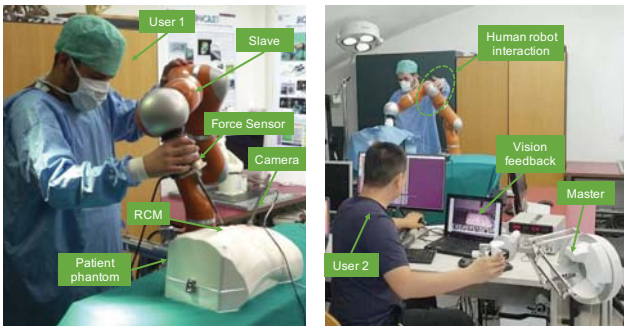

Fig. 8. Experimental setup procedures: 1) Firstly, hands-on control is utilized to allow user 1 locate the RCM constraint by hand on the patient phantom, 2) Secondly, teleoperation tracking is activated in the following procedure. User 2 uses the master to control the tool-tip tracking the virtual surgical tasks in augmented reality.

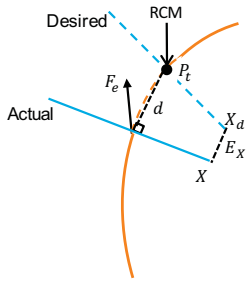

Fig. 9. Accuracy measurement. "Actual" represents the actual surgical tool shaft placement and "Desired" represents the desired surgical tool shaft placement.

$$\|\boldsymbol{F_e}\| = \sqrt{F_x^2 + F_y^2 + F_z^2} \tag{27}$$

where $\hat{\boldsymbol{u}}_{\boldsymbol{c}}$ is the actual unit direction vector of the tip pose, F_x, F_y and F_z are the 3-axis force output of the force sensor. The corresponding control coefficients table can be found in Table I. Firstly, comparison of performance between improved human-robot collaborative control strategy (IHRCC) $\boldsymbol{\tau_d = \tau_{T_1} + \tau_{T_2} + \tau_{N_{11}} + \tau_{N_{12}} + \tau_{N_2}}$ and decoupled Cartesian admittance control (DCAC) proposed by Sandoval *et al.* [6] $\boldsymbol{\tau_d = \tau_{T_1} + \tau_{N_{11}}}$ were conducted on the fixed end-effector pose. Secondly, the

performance is compared with three different teleoperation tracking tasks. All the tracking tasks are repeated for 5 trials. Fig. 10 shows the comparison of the two controllers with the same desired cartesian position and the same RCM constraint. The DCAC was applied first and then the IHRCC was switched online. Fig. 10(a) shows the swivel motion ψ with the human-robot interaction. The online Cartesian position error is shown in Fig. 10(b) and the online RCM constraint error is in Fig. 10(c). Fig. 10(d) shows the magnitude of the interaction force $\boldsymbol{F_e}$ on the abdominal wall. It is easy to see that the proposed IHRCC can constrain the swivel boundary in a safe area $[\psi_{minf}, \psi_{maxf}]$. Furthermore, the online Cartesian error and RCM constraint error converges to a smaller area. Compared with the DCAC, $\|\boldsymbol{F_e}\|$ is also constrained intro a small area.

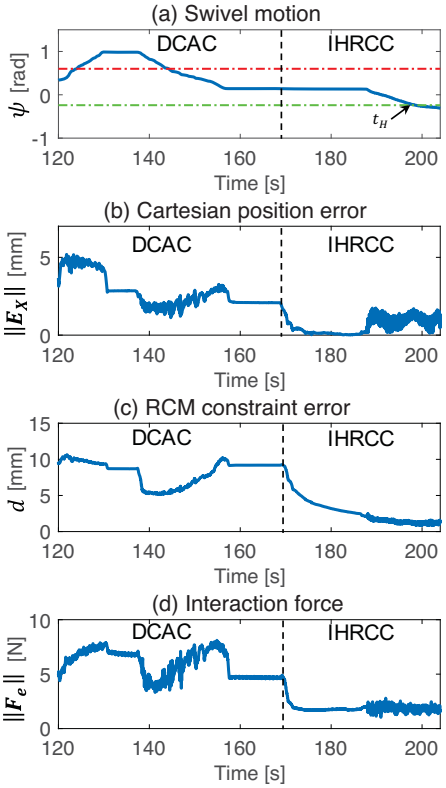

Fig. 10. Performance comparison with fixed pose between DCAC and IHRCC during human-guided swivel motion, hand force is applied by the human user on the robot arm but resisted by the robot from t_H.

Fig. 11(a) shows the corresponding error distribution of $\boldsymbol{E_X}$. Fig. 11(b) shows the corresponding error distribution of d. Since the surgical task is with the virtual trajectory in augmented reality, there is no interaction force on the surgical tip. The force is exerted on the abdominal wall by the tool shaft. Fig. 11(c) shows the corresponding distribution of interaction force $\|\boldsymbol{F_e}\|$ between the tool shaft and the abdominal wall during the teleoperation tracking. By comparison with DCAC, the accuracy of the surgical tip is improved, while the error of the RCM constraint and the interaction forces are converged into a smaller range.

IV. Discussion and Conclusion

This paper introduces a method for improved human-robot collaborative control for the teleoperated MIS. The results show that the proposed control algorithm not only can achieve the surgical task with RCM constraint but also can constrain the compliant null-space motion in a safe area and compensate the time-varying disturbance generated by the interaction, securing the quality of the surgery.

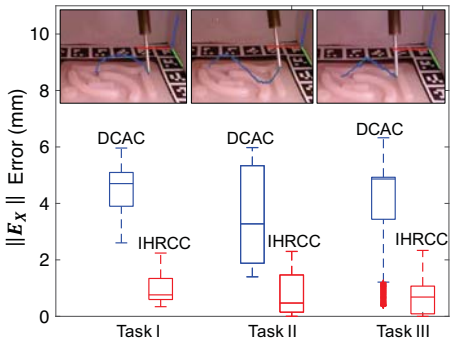

(a) Distribution of end-effector error $\|\boldsymbol{E_X}\|$

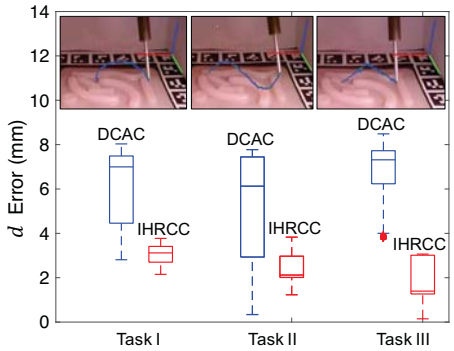

(b) Distribution of RCM constraint error d

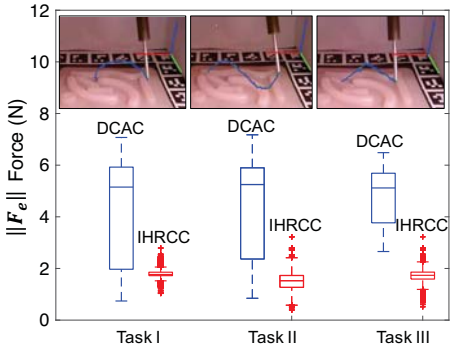

(c) Distribution of interaction force $\|\boldsymbol{F_e}\|$ on the RCM constraint

Fig. 11. Comparison between DCAC and IHRCC.

Compared to the method proposed by Sandoval *et al.* [6], the surgical task accuracy is improved, the RCM constraint and interaction force are constrained into a smaller area. Compared

with our previous work [9][14], not only the surgical task accuracy and RCM constraint are improved, but also the computation efficiency is improved without online trajectory planning. The surgeons can move the surgical arm during the ongoing surgery and the force imposed on the abdominal wall are decreased, providing flexible workspace and lower the risks for enlarging the small incision on the abdominal wall. The interaction force between the tool shaft and the abdominal wall around 1N is acceptable without hurting the small incision [36]. And the experimental evaluation is for a feasibility study of the proposed method with a proof of concept. More subjects and a through experimental validation will be conducted to verify its performance. And a more sophisticated testing setup (adding one more force sensor for external forces sensing) will be conceived and performed with the physical interaction between the surgical tip and the organs).

References

[1] N. Aghakhani, M. Geravand, N. Shahriari, M. Vendittelli, and G. Oriolo, "Task control with remote center of motion constraint for minimally invasive robotic surgery," in *Robotics and Automation (ICRA), 2013 IEEE International Conference on*. IEEE, 2013, pp. 5807–5812.

[2] R. C. Locke and R. V. Patel, "Optimal remote center-of-motion location for robotics-assisted minimally-invasive surgery," in *Robotics and Automation, 2007 IEEE International Conference on*. IEEE, 2007, pp. 1900–1905.

[3] H. Azimian, R. V. Patel, and M. D. Naish, "On constrained manipulation in robotics-assisted minimally invasive surgery," in *Biomedical Robotics and Biomechatronics (BioRob), 2010 3rd IEEE RAS and EMBS International Conference on*. IEEE, 2010, pp. 650–655.

[4] C.-H. Kuo and J. S. Dai, "Robotics for minimally invasive surgery: a historical review from the perspective of kinematics," in *International symposium on history of machines and mechanisms*. Springer, 2009, pp. 337–354.

[5] U. Hagn, R. Konietschke, A. Tobergte, M. Nickl, S. Jörg, B. Kübler, G. Passig, M. Gröger, F. Fröhlich, U. Seibold *et al.*, "Dlr mirosurge: a versatile system for research in endoscopic telesurgery," *International journal of computer assisted radiology and surgery*, vol. 5, no. 2, pp. 183–193, 2010.

[6] J. Sandoval, G. Poisson, and P. Vieyres, "Improved dynamic formulation for decoupled cartesian admittance control and rcm constraint," in *Robotics and Automation (ICRA), 2016 IEEE International Conference on*. IEEE, 2016, pp. 1124–1129.

[7] H. Su, J. Sandoval, P. Vieyres, G. Poisson, G. Ferrigno, and E. De Momi, "Safety-enhanced collaborative framework for tele-operated minimally invasive surgery using a 7-dof torque-controlled robot," *International Journal of Control, Automation and Systems*, vol. 16, no. 6, pp. 2915–2923, 2018.

[8] T. Ortmaier and G. Hirzinger, "Cartesian control issues for minimally invasive robot surgery," in *Intelligent Robots and Systems, 2000.(IROS 2000). Proceedings. 2000 IEEE/RSJ International Conference on*, vol. 1. IEEE, 2000, pp. 565–571.

[9] H. Su, J. Sandoval, M. R. Makhdoomi, G. Ferrigno, and E. De Momi, "Safety-enhanced human-robot interaction control of redundant robot for teleoperated minimally invasive surgery," in *International Conference on Robotics and Automation*, 2018, pp. 6611–6616.

[10] M. A. Peshkin, "Programmed compliance for error corrective assembly," *IEEE Transactions on Robotics and Automation*, vol. 6, no. 4, pp. 473–482, 1990.

[11] F. Petit, A. Dietrich, and A. Albu-Schäffer, "Generalizing torque control concepts: using well-established torque control methods on variable stiffness robots," *IEEE Robotics and Automation Magazine*, vol. 22, no. 4, pp. 37–51, 2015.

[12] M. D. Comparetti, E. De Momi, A. Vaccarella, M. Riechmann, and G. Ferrigno, "Optically tracked multi-robot system for keyhole neurosurgery," in *Robotics and Automation (ICRA), 2011 IEEE International Conference on*. IEEE, 2011, pp. 661–666.

[13] H. Su, N. Enayati, L. Vantadori, A. Spinoglio, G. Ferrigno, and E. De Momi, "Online human-like redundancy optimization for tele-operated anthropomorphic manipulators," *International Journal of Advanced Robotic Systems*, vol. 15, no. 6, p. 1729881418814695, 2018.

[14] J. Sandoval, H. Su, P. Vieyres, G. Poisson, G. Ferrigno, and E. De Momi, "Collaborative framework for robot-assisted minimally invasive surgery using a 7-dof anthropomorphic robot," *Robotics and Autonomous Systems*, vol. 106, pp. 95–106, 2018.

[15] H. Su, G. Ferrigno, and E. De Momi, "Adaptive decoupling control of a serial redundant robot for teleoperated minimally invasive surgery," in *IEEE ICRA Workshop on Supervised Autonomy in Surgical Robotics*, 2018.

[16] H. Su, H. Zhang, Z. Li, and C.-Y. Su, "Adaptive fuzzy control of operation space constrained exoskeletons under unmodelled dynamics," in *Intelligent Control and Automation (WCICA), 2014 11th World Congress on*. IEEE, 2014, pp. 3277–3282.

[17] Z. Li, C.-Y. Su, G. Li, and H. Su, "Fuzzy approximation-based adaptive backstepping control of an exoskeleton for human upper limbs," *IEEE Transactions on Fuzzy Systems*, vol. 23, no. 3, pp. 555–566, 2015.

[18] A. M. Dietrich, "Whole-body impedance control of wheeled humanoid robots," Ph.D. dissertation, Technische Universität München, 2015.

[19] A. Dietrich, C. Ott, and J. Park, "The hierarchical operational space formulation: Stability analysis for the regulation case," *IEEE Robotics and Automation Letters*, vol. 3, no. 2, pp. 1120–1127, 2018.

[20] L. Sciavicco and B. Siciliano, *Modelling and control of robot manipulators*. Springer Science & Business Media, 2012.

[21] O. Khatib, "A unified approach for motion and force control of robot manipulators: The operational space formulation," *IEEE Journal on Robotics and Automation*, vol. 3, no. 1, pp. 43–53, 1987.

[22] C. Ott, "Cartesian impedance control: The rigid body case," in *Cartesian Impedance Control of Redundant and Flexible-Joint Robots*. Springer, 2008, pp. 29–44.

[23] J. Baillieul, "Kinematic programming alternatives for redundant manipulators," in *Robotics and Automation. Proceedings. 1985 IEEE International Conference on*, vol. 2. IEEE, 1985, pp. 722–728.

[24] A. Dietrich, *Whole-body impedance control of wheeled humanoid robots*. Springer, 2016.

[25] L. Jin, S. Li, H. M. La, and X. Luo, "Manipulability optimization of redundant manipulators using dynamic neural networks," *IEEE Transactions on Industrial Electronics*, vol. 64, no. 6, pp. 4710–4720, June 2017.

[26] M. Shimizu, H. Kakuya, W.-K. Yoon, K. Kitagaki, and K. Kosuge, "Analytical inverse kinematic computation for 7-dof redundant manipulators with joint limits and its application to redundancy resolution," *IEEE Transactions on Robotics*, vol. 24, no. 5, pp. 1131–1142, 2008.

[27] J. Humphrey and C. Taylor, "Intracranial and abdominal aortic aneurysms: similarities, differences, and need for a new class of computational models," *Annu. Rev. Biomed. Eng.*, vol. 10, pp. 221–246, 2008.

[28] E. Peña, B. Hernández-Gascón, and B. Calvo, "Human abdomen: Mechanical modeling and clinical applications," in *Biomechanics of Living Organs*. Elsevier, 2017, pp. 267–285.

[29] H. Su, Z. Li, G. Li, and C. Yang, "Emg-based neural network control of an upper-limb power-assist exoskeleton robot," in *International Symposium on Neural Networks*. Springer, 2013, pp. 204–211.

[30] S. Tong and Y. Li, "Adaptive fuzzy output feedback control of mimo nonlinear systems with unknown dead-zone inputs," *IEEE Transactions on Fuzzy Systems*, vol. 21, no. 1, pp. 134–146, 2013.

[31] S. Tong, Y. Li, and P. Shi, "Observer-based adaptive fuzzy backstepping output feedback control of uncertain mimo pure-feedback nonlinear systems," *IEEE Transactions on Fuzzy Systems*, vol. 20, no. 4, pp. 771–785, 2012.

[32] L.-X. Wang, "Stable adaptive fuzzy control of nonlinear systems," *IEEE Transactions on fuzzy systems*, vol. 1, no. 2, pp. 146–155, 1993.

[33] G. Schreiber, A. Stemmer, and R. Bischoff, "The fast research interface for the kuka lightweight robot," in *IEEE Workshop on Innovative Robot Control Architectures for Demanding (Research) Applications How to Modify and Enhance Commercial Controllers (ICRA 2010)*, 2010, pp. 15–21.

[34] N. Enayati, "Adaptive shared-control in surgical robotics," Ph.D. dissertation, Politecnico di Milano, 2017.

[35] N. Enayati, A. M. Okamura, A. Mariani, E. Pellegrini, M. M. Coad, G. Ferrigno, and E. De Momi, "Robotic assistance-as-needed for enhanced visuomotor learning in surgical robotics training: An experimental study," in *2018 IEEE International Conference on Robotics and Automation (ICRA)*. IEEE, 2018, pp. 6631–6636.

[36] B. Böhm, M. Knigge, M. Kraft, K. Gründel, and U. Boenick, "Influence of different trocar tips on abdominal wall penetration during laparoscopy," *Surgical endoscopy*, vol. 12, no. 12, pp. 1434–1438, 1998.